Nuclear Magnetic Resonance Investigations of Calcium-antagonist Drugs. Part 1. Conformational and Dynamic Features of Nimodipine {3-[(2-Methoxyethoxy)carbonyl]-5-(isopropoxycarbonyl)-4-(3-nitrophenyl)-2,6-dimethyl-1,4-dihydropyridine} in [$^2H_6$]Dimethyl Sulphoxide

Elena Gaggelli, Nadia Marchettini, and Gianni Valensin
Department of Chemistry, University of Siena, Pian dei Mantellini 44, 53100 Siena, Italy

Conformational and dynamic features of nimodipine in [$^2H_6$]DMSO solution were investigated by 1D and 2D n.m.r. techniques. ^1H and ^{13}C n.m.r. relaxation rates, ^{13}C-{^1H} n.O.e.s, and 2D n.O.e. proton spectra were used to build up a Dreiding model of the preferred conformation. Folding of the two side-chains in opposite directions was indicated. Complete anisotropic motion was assumed wherefrom internal reorientational times within the phenyl ring and the side-chains were evaluated. Folding of the isopropoxycarbonyl side-chain was also demonstrated by motional constraints undergone by carbon atoms within it.

Nimodipine {3-[(2-methoxyethoxy)carbonyl]-5-(isopropoxycarbonyl)-4-(3-nitrophenyl)-2,6-dimethyl-1,4-dihydropyridine} (see Figure 1) is a drug which interacts with the voltage-sensitive calcium channel (calcium-antagonists or calcium-entry blockers). Such drugs display astonishing variety in chemical structure and pharmacological activity.[1] While dihydropyridines act at a nitrendipine receptor, diphenylalkylamines (*e.g.* verapamil) act on a second distinct receptor, linked to the first one, inhibiting binding of nitrendipine, and benzothiazepines (*e.g.* diltiazem) act on a third receptor, increasing the binding of nitrendipine.

The diverse chemical structures and biological activities, together with the variety of therapeutic actions, have prompted extensive research on molecular mechanisms of action as well as on conformational features.[2–4]

Much information can be gained by investigating the preferred conformation in solution and the effect on conformational equilibria of the presence of (i) divalent metal ions, especially Ca^{II} or the calcium-mimicking Mn^{II}, and (ii) macromolecular receptors either in the presence or absence of metal ions. These points can be approached by n.m.r. techniques that provide a direct knowledge of dipole–dipole interactions in solution wherefrom relevant structural and dynamic features can be inferred. Homo- and hetero-nuclear dipole–dipole interactions can be quantified from selective relaxation rate measurements,[5] nuclear Overhauser effects (n.O.e.s),[6] and 2D magnetization transfer experiments.[7,8]

In this paper we report ^1H and ^{13}C n.m.r. measurements on nimodipine in solution with the aim of delineating conformational and dynamic features relevant for molecular mechanisms.

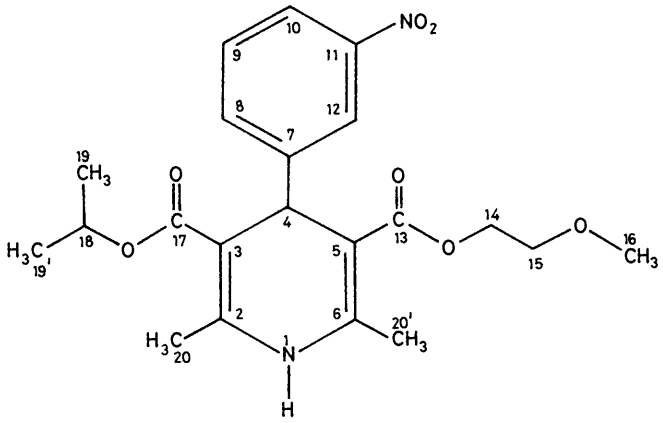

Figure 1. Molecular formula and numbering scheme of nimodipine

Experimental

Nimodipine was supplied by Janssen Pharmaceutica (Beerse, Belgium) and used without further purification. Solutions were made in 99.96% [$^2H_6$]DMSO (Merck) and were carefully deoxygenated.

N.m.r. spectra were taken on a Varian XL-200 spectrometer in the pulse-Fourier transform mode at probe temperatures of 25 ± 1 °C; chemical shifts were referenced to the ^1H and ^{13}C resonances of internal tetramethylsilane. ^1H and ^{13}C spectra were measured with 5 mm and 10 mm o.d. sample tubes respectively. Non-selective spin–lattice relaxation rates were measured with the inversion recovery pulse sequence $(t–\pi–\tau–\pi/2)_n$; 4 and 100 f.i.d.s were collected for ^1H and ^{13}C T_1 experiments respectively. Spin–spin relaxation rates were measured with the Carr–Purcell–Meiboom–Gill pulse sequence. $1/T_1$ $(=R_1)$ or $1/T_2$ $(=R_2)$ values were calculated from exponential regression analysis of the recovery or decay curves of longitudinal or transverse magnetization components by using a computer attached to the spectrometer.

Selective proton spin–lattice relaxation rates were measured with inversion recovery pulse sequences where the π pulse was given by the proton decoupler at the selected frequency for relatively long times at low power. The $\pi/2$ pulse was, on the other hand, the usual non-selective $\pi/2$ pulse given by the proton transmitter. The R^s values were measured in the initial slope approximation.[5]

2D n.O.e. proton spectra were measured by using pulse sequences described in refs. 7 and 8. The spectral width was 2 000 Hz, and the data set consisted of 512 points in the t_1 dimension and 1 024 points in the t_2 dimension. 16 free induction decays were accumulated for each value of t_1 and the total accumulation time was *ca.* 4 h.

^{13}C-{^1H} n.O.e.s were measured with gated decoupling techniques. Selective ^{13}C-{^1H} n.O.e.s were determined by applying a 10 s low-power saturating pulse at the appropriate peak position, immediately followed by a high-power $\pi/2$ observing pulse. The presaturating pulse was chosen long enough to allow establishment of Overhauser equilibrium. Off-resonance control spectra were measured with the presaturating pulse offset 1000 Hz to low field.

Table 1. 200 MHz ^{1}H N.m.r. parameters of nimodipine (0.2 mol dm^{-3}) in [$^2H_6$]DMSO at *T* 293 K

Resonance	δ	R_1^{ns}/s^{-1}	R_1^{s}/s^{-1}	R_2/s^{-1}
NH	9.0	3.533	3.048	7.519
10-, 12-H	8.0	0.833	0.672	2.667
8-, 9-H	7.5	1.368	1.160	3.067
4-H	4.9	1.144	0.864	2.785
18-H	4.8	0.726	0.677	13.698
14-H	4.0	2.326		3.846
15-H	3.4	2.778		4.082
16-H	3.2	0.683		2.519
20-, 20′-H	2.3	2.437		5.181
19-H	1.2	1.941		5.848
19′-H	1.0	1.941		5.848

R_1^{ns} = non-selective longitudinal relaxation rate; R_1^{s} = selective longitudinal relaxation rate; R_2 = spin–spin relaxation rate.

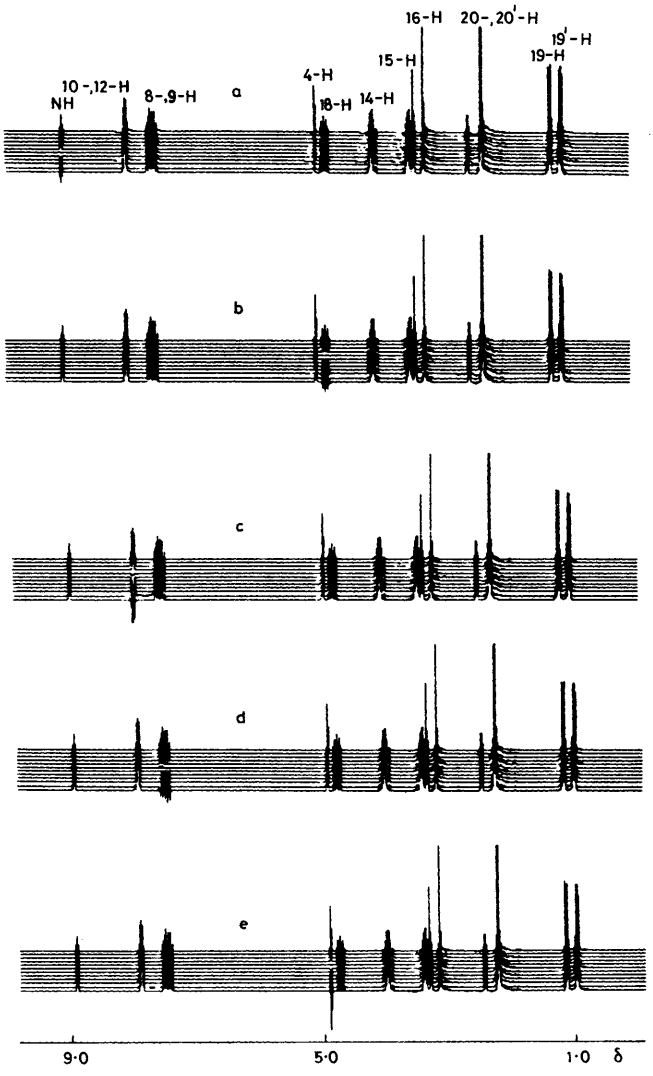

Figure 2. Typical selective proton spin–lattice relaxation rate measurements for selected protons of nimodipine (0.2 mol dm^{-3}) in [$^2H_6$]DMSO at 293 K

Results

The ^{1}H n.m.r. parameters of nimodipine in [$^2H_6$]DMSO solution are reported in Table 1. Spectral assignment was achieved by homonuclear spin decoupling and by reference to

Table 2. ^{13}C N.m.r. chemical shifts, longitudinal relaxation rates, nuclear Overhauser effects (n.O.e. = I_z/I_0), and motional correlation times for nimodipine (0.2 mol dm^{-3}) in [$^2H_6$]DMSO at 293 K

Resonance	δ (p.p.m.)	R_1/s^{-1}	N.O.e.	$10^{10}\ \tau_c/s$
C-13	178.5	0.141	2.18	
C-17	178.1	0.131	2.12	
C-7	161.4	0.145	2.17	
C-11	157.6	0.136	2.22	
C-3	157.1	0.289	2.27	
C-5	156.2	0.162	1.99	
C-8	143.5	2.457	2.73	1.21
C-9	138.3	2.544	2.80	1.25
C-12	130.0	2.227	2.80	1.09
C-10	128.5	2.994	2.98	1.47
C-2	107.6	0.180	2.19	
C-6	106.6	0.152	1.98	
C-15	72.8	2.202	2.85	0.54
C-18	69.0	1.335	2.79	0.66
C-14	64.7	2.494	2.77	0.61
C-16	60.0	0.252	2.81	0.04
C-4	34.7	2.347		1.15
C-19	20.4	1.038	2.98	0.27
C-19′	19.7	1.132	2.81	0.26
C-20, -20′	15.7	0.922	2.83	0.15

τ_c Was calculated by Allerhand's formula (6).

Table 3. Nuclear Overhauser effects (n.O.e. = I_z/I_0) upon selective irradiation of 4-H of nimodipine (0.2 mol dm^{-3}) in [$^2H_6$]DMSO at 293 K and calculated distances

Resonance	N.O.e.	*r*/Å
C-7	1.33	2.20
C-14	1.12	1.62
C-15	1.06	1.92
C-16	1.07	2.57

data in the literature. Typical selective irradiation experiments are shown in Figure 2 from which selective proton spin–lattice relaxation rates were calculated as summarized in Table 1 where non-selective spin–lattice and spin–spin relaxation rates are also reported. The n.O.e. spectrum is shown in Figure 3 where the 1D ^{1}H n.m.r. spectrum is superimposed for reference in both frequency dimensions. If compared with the intensity of the corresponding diagonal peaks at zero mixing times, the intensities of cross-peaks were in the range 15—19%, demonstrating that 250 ms was very close to the optimum mixing time.[9] Strong dipolar connectivities are manifest in the 2D spectrum between 18- and 20-H and also between 20-H and both 19- and 19′-H, although one of them is much stronger than the other.

The ^{13}C n.m.r. parameters are reported in Table 2. Spectral assignment was achieved by using the attached proton test,[10] followed by selective decoupling experiments and was ratified by 2D ^{1}H and ^{13}C chemical shift correlation spectra. Spin–lattice relaxation rates and ^{13}C-{^{1}H} n.O.e.s are also summarized in Table 2 together with a value for the correlation time modulating the corresponding ^{13}C-^{1}H interaction, as calculated by Allerhand's formula.[11] Presaturation of the 4-H resonance with a soft pulse as long as or longer than $10T_1$ of C-4 was employed with the aim of observing the selective ^{13}C-{^{1}H} Overhauser enhancements in Table 3 and shown to allow extraction of relevant geometrical features.

Discussion

As far as molecular dynamics is concerned ^{1}H n.m.r. relaxation investigations are usually neglected. In fact, such relaxation

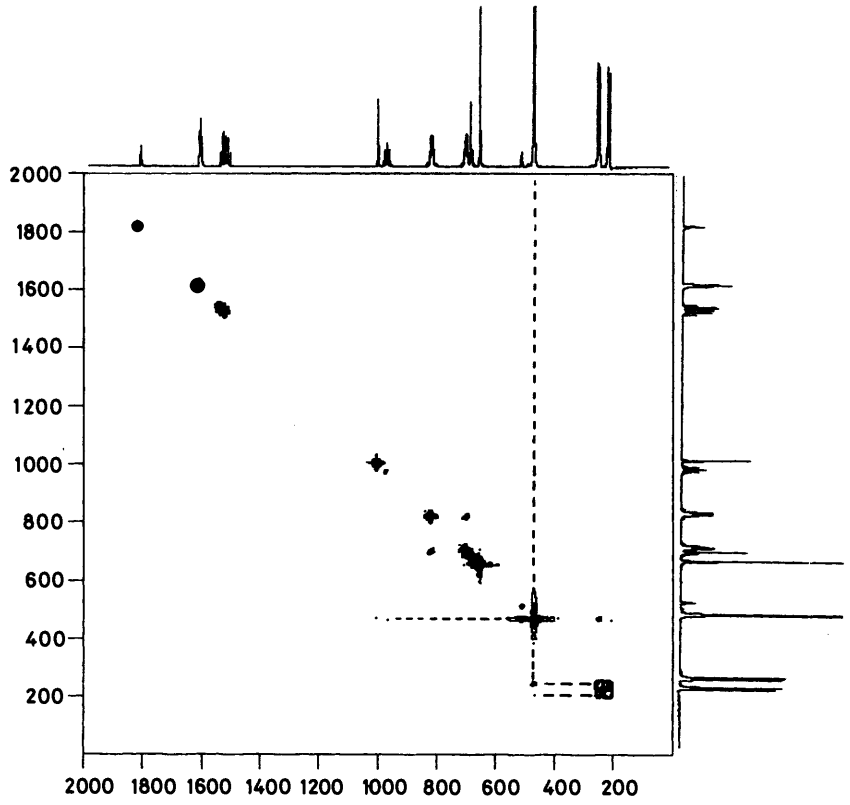

Figure 3. Contour plot of the 2D n.O.e. spectrum at 200 MHz of nimodipine (0.2 mol dm^{-3}) in [$^2H_6$]DMSO (degassed). The mixing time was 200 ms. Dashed lines show dipolar connectivities between protons of the isopropoxycarbonyl chain and the methyls attached to the dihydropyridine ring. (See Experimental section for further details)

rates, usually measured by means of strong radiofrequency pulses that excite the whole ^1H spectrum, contain an intriguing variety of relaxation mechanisms involving several relaxation vectors. In fact the deviations of the energy-level populations from equilibrium are governed by rate equations that yield equation (1) for any spin i.[5] In equation (1) $(I_{zi} - I_{0i})$ and

$$d/dt(I_{zi} - I_{0i}) = -\left(\sum_{i \neq j} \rho_{ij} + \rho_{i^*}\right)(I_{zi} - I_{0i}) - \sum_{i \neq j} \sigma_{ij}(I_{zj} - I_{0j}) \quad (1)$$

$(I_{zj} - I_{0j})$ are deviations from equilibrium population differences, ρ_{ij} and σ_{ij} are the direct and cross-relaxation terms, respectively, for any i–j spin pair, ρ_{i^*} accounts for mechanisms other than dipolar, and the sums are extended to all the effective i—j proton pairs.

After a non-selective 180° excitation the initial rate constant for recovery of longitudinal magnetization is given by equation (2).[5] Since each i–j pair is likely to be characterized by its own

$$R_i^{ns} = \sum_{i \neq j} \rho_{ij} + \rho_{i^*} + \sum_{i \neq j} \sigma_{ij} \quad (2)$$

^1H–^1H distance and motional correlation time, even in the most fortunate case of a 100% contribution from ^1H–^1H dipolar interactions ($\rho_i^* 0$), it is usually quite hard to extract structural and/or motional features from such 'non-selective' ^1H n.m.r. relaxation rate measurements.

As a consequence the non-selective relaxation rates (Table 1) can only be used to assess general and qualitative properties. It is for example evident that the ratio between R_2 and R_1 is much greater than 1, such that a unique correlation time cannot be used for a description of the motion of relexation vectors. Occurrence of motions diverse and much slower than those determining the spin–lattice relaxation rate is likely better to explain the observed ratios in the light of ^{13}C n.m.r. data which yield evidence of motional correlation times well within the extreme narrowing region. This being the case, it is apparent that slow motions provide very efficient contributions to the spin–spin relaxation rate of 18-H.

However if only narrow regions of the ^1H n.m.r. spectrum (see Figure 2) are selectively excited by 'soft' radiofrequency pulses, the interpretation of relaxation rate data is much more straightforward. In fact all the σ_{ij} values involving protons outside the excited region are cancelled out and the relaxation rate equation, in the initial rate approximation, is simplified to (3). If 'non-selective' and 'selective' relaxation rates are

$$R_i^s = \sum_{i \neq j} \rho_{ij} \quad (3)$$

compared, σ or ρ terms for single proton pairs can be extracted. This is the case if we consider the selective spin–lattice relaxation rate measured after irradiation of 8- and 9-H (spectrum d in Figure 2). The only σ term left in the equation for such selective relaxation rate is that for the mutual 8-H–9-H dipole–dipole interaction [equation (4)].

$$R^s_{8,9} = \sum_{i \neq j} \rho_{ij} + \sigma_{8,9} \quad (4)$$

On the other hand the non-selective relaxation rate has contributions by σ terms other than $\sigma_{8,9}$. If the reasonable assumption is made that the difference between $R^{ns}_{8,9}$ and $R^s_{8,9}$

is due only to $\sigma_{9,10}$ ($\sigma_{8,10}$, $\sigma_{9,12}$, and $\sigma_{8,12}$ are negligibly small because of their dependence upon r_{ij}^{-6}), then equations (5) will

$$\sigma_{9,10} = R^{ns}_{8,9} - R^{s}_{8,9} = 0.208\ s^{-1} \quad (5)$$

hold. As the distance 8-H–9-H is known from neutron scattering data (r 2.44 Å), the correlation time of motion modulating reorientation of the relaxation vector can be consequently calculated (τ_c 1.64 ± 0.20 × 10^{-10} s at 293 K).

Further motional features were obtained by considering ^{13}C n.m.r. spin–lattice relaxation rates. In this case relaxation equations are considerably simplified since only the dipolar interaction with directly bound protons usually determines the relaxation mechanism, as also demonstrated, in our case, by the very high ^{13}C-{^1H} n.O.e.s measured for protonated carbons (Table 2). However, ^{13}C spin–lattice relaxation rates can be interpreted in terms of rotational diffusion coefficients provided molecular motions can be fitted to a physical model based on intuition or experiment. This is not likely to apply to our case where overall anisotropic motion with several degrees of internal motion is expected. It is nonetheless still possible to gain qualitative information by calculating the reorientational correlation times for each ^{13}C–^1H relaxation vector with equation (6) of Allerhand *et al.*[11] where n_H is the number of

$$R_1 = n_H \times 2.0235 \times 10^{10}\ \tau_c \quad (6)$$

protons attached to the carbon atom under consideration (see Table 2). Such reorientational times show that (i) the C-7–C-10 axis is the main rotational axis for the phenyl ring; (ii) the reorientational time for the C-7–C-10 axis is longer than the correlation time for modulation of the 8-H–9-H relaxation vector, suggesting that rotation around the axis is not the slowest motion within the molecule; (iii) the reorientational time of the C-4–4-H relaxation vector is similar to those of C–H vectors within the aromatic ring and much shorter than that of the 8-H–9-H vector; and (iv) C–H vectors within the side-chains reorient much more freely than those within the rings, but the methyls of the isopropoxy group and those attached to the dihydropyridine ring are somehow more hindered than the methyl of the methoxyethoxy side-chain.

The reasons why the isopropoxycarbonyl side-chain undergoes hindered motion were investigated by measuring the ^1H–^1H dipole–dipole connectivities obtained from a 2D n.O.e. magnetization transfer experiment (Figure 3). The out-of-diagonal contours represent connectivities between protons that exchange longitudinal magnetization, through dipolar coupling, during the mixing time. Since the interaction energy depends upon r^{-6}, thus decaying very rapidly with increasing distance, only nearby protons, within a range of *ca.* 4—5 Å, are expected to show up as exchanging pairs. As shown in Figure 3, interesting dipolar interactions are measured between methyls attached to the dihydropyridine ring and both methine and methyls of the isopropoxycarbonyl moiety, suggesting that this side-chain is folded towards the dihydropyridine ring. Steric hindrance can therefore be claimed as the main reason for the relatively slow motion obtained from measurements of ^{13}C spin–lattice relaxation rates.

Delineation of conformational features was completed by measuring ^{13}C-{^1H} n.O.e. within the (2-methoxyethoxy)-carbonyl side-chain upon selective irradiation of 4-H. It is in fact known that presaturation of any proton H_x dipolarly coupled to any carbon C_y generates an n.O.e. given by equation (7),[6,12] where R_{C_y} is the spin–lattice relaxation rate measured

$$f_{C_y}\{H_x\} = \frac{\gamma_H(W_2 - W_0)}{\gamma_C R_{C_y}} = \frac{f(\tau_c)}{r^6_{H_xC_y}} R^{-1}_{C_y} \quad (7)$$

for C_y under broadband decoupling conditions and W_2 and W_0 are the double- and zero-quantum dipolar relaxation transition probabilities, respectively, based on the distance $r_{H_xC_y}$ and on the motional correlation time for modulation of reorientation of the C_y–H_x relaxation vector. In consequence, if saturation of any proton resonance H_x yields a detectable n.O.e. on more than one carbon atom, knowledge of the C_y–H_x distance allows evaluation of all the other C_z–H_x distances, provided the same $f(\tau_c)$ describes motions of the various C–H vectors [equation (8)].[12] By assuming $r_{C\text{-}4,H\text{-}4}$ 1.05 Å, several distances could be

$$\sqrt[6]{\frac{f_{C_y}\{H_x\}R_{C_y}}{f_{C_z}\{H_x\}R_{C_z}}} = \frac{r_{C_zH_x}}{r_{C_yH_x}} \quad (8)$$

calculated by measuring the ^{13}C-{H-4} n.O.e.s on C-7, -14, -15, -16, as reported in Table 3. The calculated distances are approximate values since the same $f(\tau_c)$ was assumed in every case, which is not likely, but provide a good quantitative approach for delineation of interesting conformational features. The validity of the approach is, in fact, demonstrated by the measured value of 2.20 Å for the C-7–H-4 distance which is a constant parameter. It can be therefore stated that the C-13–C-16 side-chain folds back in a way that brings 14- and 15-CH_2 in proximity to 4-H and, hence, that the two side-chains fold in opposite directions.

Conclusions.—The conformation assumed by nimodipine in solution is shown in Figure 4 as a projection of the Dreiding model built up on the basis of n.m.r. parameters only. This conformation should not be considered as a rigid one corresponding to the minimum-energy conformation. Dynamics in solution yield evidence of a high degree of flexibility of the two side-chains. However, H^1-{^1H} and ^{13}C-{^1H} n.O.e.s demonstrate that the two substituents fold in opposite directions and that molecular motions affect atoms within the flexible chains at a relatively short distance from the ring. The conformation inferred from n.O.e. data is therefore to be taken as one of several conformations differing in the relative position of the carbon atoms within the side-chains.

The following features can be outlined. The aromatic ring is out of the plane in the axial position; the isopropoxycarbonyl chain folds back and 18-, 19′-, and 19-H are brought into

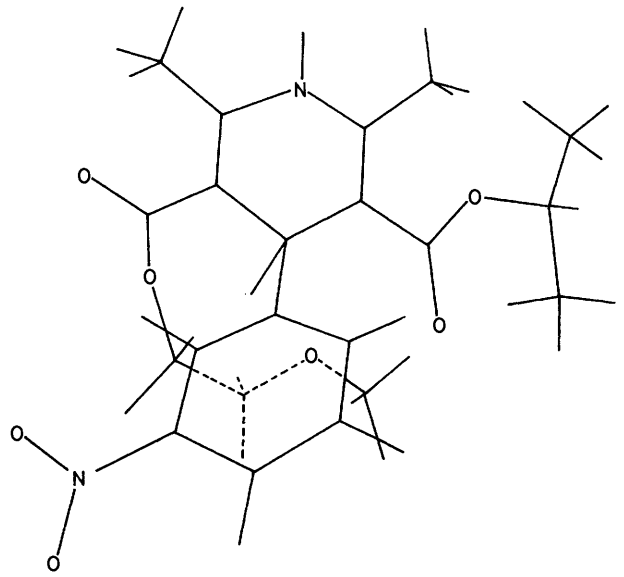

Figure 4. Projection of the Dreiding model of the preferred conformation of nimodipine in [$^2H_6$]DMSO

proximity to 20-H by internal motion; the (2-methoxyethoxy)-carboxyl chain folds back in the opposite direction such that C-14, -15, and -16 are close enough to 4-H to account for the observed ^{13}C-{H-4} n.O.e. Folding of this chain indicates that the axial rather than the equatorial position is preferred by the phenyl ring. With the phenyl ring in the equatorial position, it is in fact not possible for both 14- and 15-CH_2 to be close to 4-H. It should, however, be recognized that relatively slow equatorial–axial interconversion is likely. This kind of motion is, moreover, the only slow reorientational motion that can account for the observed spin–spin relaxation.

From the dynamic point of view, molecular motion is completely anisotropic: rotation of the phenyl ring around the C-7–C-10 axis is somehow faster than reorientation of 8-H–9-H relaxation vector. Since rotation around C-7–C-10 does not modulate the H-8–H-9 dipolar interaction, the corresponding correlation time (τ_c 1.64×10^{-10} s) may be assumed as the backbone correlation time, yielding τ_c 1.47×10^{-10} s for rotation of the C-7–C-10 axis and τ_c 1.21×10^{-10} s for librational motion around the axis. The two side-chains have additional degrees of freedom but motion in the isopropoxy-carbonyl moiety is impeded by steric hindrance by the dihydropyridine ring.

References

1 S. H. Snyder and I. J. Reynolds, *New England J. Med.*, 1985, **313**, 995.
2 A. M. Triggle, E. Shefter, and D. J. Triggle, *J. Med. Chem.*, 1980, **23**, 1442.
3 R. Fossheim, K. Swarteng, A. Mostad, C. Romming, E. Shefter, and D. J. Triggle, *J. Med. Chem.*, 1982, **25**, 126.
4 D. A. Langs and D. J. Triggle, *Mol. Pharmacol.*, 1985, **27**, 544.
5 R. Freeman, H. D. W. Hill, B. L. Tomlinson, and L. D. Hall, *J. Chem. Phys.*, 1974, **61**, 4466.
6 J. H. Noggle and R. E. Schirmer, 'The Nuclear Overhauser Effect,' Academic Press, New York, 1971.
7 A. Kumar, R. R. Ernst, and K. Wüthrich, *Biochem. Biophys. Res. Commun.*, 1980, **95**, 1.
8 A. Kumar, G. Wagner, R. R. Ernst, and K. Wüthrich, *Biochem. Biophys. Res. Commun.*, 1980, **96**, 1156.
9 S. Macura and R. R. Ernst, *Mol. Phys.*, 1980, **41**, 95.
10 C. LeCocq and J.-Y. Lallemand, *J. Chem. Soc., Chem. Commun.*, 1981, 150.
11 A. Allerhand, D. Doddrell, and R. Komoroski, *J. Chem. Phys.*, 1971, **55**, 189.
12 N. Niccolai, C. Rossi, P. Mascagni, P. Neri, and W. A. Gibbons, *Biochem. Biophys. Res. Commun.*, 1984, **124**, 739.

Received 16*th June* 1986; *Paper* 6/1210